PERGAMON

Mechanics Research Communications 30 (2003) 161–174

MECHANICS
RESEARCH COMMUNICATIONS

www.elsevier.com/locate/mechrescom

A new concept of modal participation factor for numerical instability in the dual BEM for exterior acoustics

J.T. Chen [a], K.H. Chen [a], I.L. Chen [b,*], L.W. Liu [c]

[a] *Department of Harbor and River Engineering, National Taiwan Ocean University, P.O. Box 7-59, Keelung 20224, Taiwan*
[b] *Department of Naval Architecture, National Kaohsiung Institute of Marine Technology, Kaohsiung 811, Taiwan*
[c] *Department of Civil Engineering, National Taiwan University, Taipei 106, Taiwan*

Received 23 March 2001

Abstract

This paper presents the occurring mechanism why irregular frequencies are imbedded in the exterior acoustics using the dual boundary element method (BEM). The modal participation factor which dominates the numerical instability is derived for continuous and discrete systems. In addition, the irregular (fictitious) frequencies embedded in the singular or hypersingular integral equations are discussed, respectively. It is found that the irregular values depend on the kernels in the integral representation for the solution. A two-dimensional dual BEM program for the exterior acoustics was developed. Numerical experiments are conducted to verify the concept of modal participation factor.

Keywords: Modal participation factor; Fictitious frequency; Exterior acoustics; Dual BEM; Scattering

1. Introduction

Irregular frequencies, or so called fictitious frequencies for exterior acoustics in boundary element method (BEM) or boundary integral equation method (BIEM), have been studied by many researchers (Burton and Miller, 1971; Schenck, 1968) for a long time. For a continuous system, Chen (1998) proved analytically using the dual series model that the positions of fictitious frequencies depend on the kernel in the integral representation for the solution. The types of boundary condition can not change the positions where fictitious frequencies occur once the integral formulation is chosen. Later, Chen and Kuo (2000) applied the theory of circulants to understand the occurring mechanism of irregular frequencies for a discrete system by considering a circular radiator. Numerical examples for nonuniform radiation problems using the dual BEM were provided and irregular frequencies were easily found (Chen et al., 2000). Although the fictitious frequencies can be predicted theoretically (Chen, 1998; Chen and Kuo, 2000), we may not find the positions of numerical instability in the real computation for some cases. How to explain

* Corresponding author. Tel.: +886-7-3617141-3402.
E-mail address: ilchen@mail.nkimt.edu.tw (I.L. Chen).

PII: S0093-6413(02)00351-8

the reason is not trivial. Very few literature on this topic can be found to the authors' best knowledge. In structural dynamics, the concept of modal participation factor (Chen et al., 1995) is well known for structural engineers. It indicates the weighting how the corresponding mode contributes to the response. This concept can be applied to the excitations of body force, boundary force and boundary support motion. The modal participation factor for both the continuous system (Chen et al., 1996) and discrete system (Chen et al., 1995, 1997) were derived in structural dynamics.

In this paper, we will propose the concept of modal participation factor for the numerical instability in the dual BEM for exterior acoustics. A dual BEM program was implemented to examine how the modal participation factor dominates the numerical instability near the fictitious frequency. The nonzero modal participation factor causes the numerical oscillation since the total solution is contaminated by the corresponding fictitious mode. The positions of fictitious frequencies for the exterior problems using the first equation of the dual BEM (the singular integral equation—*UT* method) or the second equation of the dual BEM (the hypersingular integral equation—*LM* method) will be discussed. Four numerical examples of radiation problems and scattering problems subject to the Dirichlet and Neumann boundary conditions, will be illustrated to show how participation factor contributes numerical instability to the total solution. Numerical results using four approaches, the *UT* method, the *LM* method, the CHIEF method, the Burton and Miller method, will be verified in comparison with the analytical solutions and the DtN results (Harari et al., 1997; Stewart and Hughes, 1997). The modal participation factor for the corresponding modes will be determined to predict the contribution of the numerical instability. To circumvent the problem of numerical instability near the fictitious frequency, the Burton and Miller method (Burton and Miller, 1971) and CHIEF method (Schenck, 1968; Chen et al., 2001) will be employed for comparisons.

2. Dual formulation for two-dimensional radiation and scattering problems

The governing equation for an exterior acoustic problem is the Helmholtz equation as follows:

$$(\nabla^2 + k^2)u(x_1, x_2) = 0, \quad (x_1, x_2) \in D,$$

where u is the acoustic potential, ∇^2 is the Laplacian operator, D is the domain and k is the wave number, which is angular frequency over the speed of sound. The boundary conditions can be either the Neumann or Dirichlet type. Based on the dual formulation, the dual equations for the boundary points are

$$\pi u(x) = \mathrm{CPV}\int_B T(s,x)u(s)\,\mathrm{d}B(s) - \mathrm{RPV}\int_B U(s,x)t(s)\,\mathrm{d}B(s), \quad x \in B, \tag{1}$$

$$\pi t(x) = \mathrm{HPV}\int_B M(s,x)u(s)\,\mathrm{d}B(s) - \mathrm{CPV}\int_B L(s,x)t(s)\,\mathrm{d}B(s), \quad x \in B, \tag{2}$$

where CPV, RPV and HPV denote the Cauchy principal value, the Riemann principal value and the Hadamard principal value, $t(s) = \partial u(s)/\partial n_s$, $U(s,x)$ is the fundamental solution, (Chen, 1998)

$$T(s,x) = \frac{\partial U(s,x)}{\partial n_s}, \quad L(s,x) = \frac{\partial U(s,x)}{\partial n_x} \quad \text{and} \quad M(s,x) = \frac{\partial^2 U(s,x)}{\partial n_s \partial n_x},$$

B denotes the boundary enclosing D and the U, T, L and M are the four kernels in the dual formulation. By discretizing the boundary into boundary elements, the linear algebraic equations for the dual boundary integral equations can be written as

$$[T_{pq}]\{u_q\} = [U_{pq}]\{t_q\}, \tag{3}$$

$$[M_{pq}]\{u_q\} = [L_{pq}]\{t_q\}, \tag{4}$$

where $[U]$, $[T]$, $[L]$ and $[M]$ are the four influence matrices, $\{u_q\}$ and $\{t_q\}$ are the boundary potential and flux, and the subscripts p and q correspond to the labels of the collocation element and integration element, respectively. In order to avoid the problem of fictitious frequency, the Burton and Miller formulation (Burton and Miller, 1971) is employed by combining the dual equations as follows,

$$\left\{[T_{pq}] + \frac{i}{k}[M_{pq}]\right\}\{u_q\} = \left\{[U_{pq}] + \frac{i}{k}[L_{pq}]\right\}\{t_q\}, \tag{5}$$

where $i^2 = -1$. Also, the CHIEF method (Schenck, 1968) by adding the constraints from the interior points is considered for comparisons.

3. Modal participation factor for numerical instability—continuous system

For simplicity, we propose the concept of modal participation factor by a circular case. By expanding the four kernels in the dual formulation, we have the following degenerate kernels,

$$U(s,x) = \begin{cases} U^i(R,\theta;\rho,\phi) = \sum_{m=-\infty}^{\infty} \frac{\pi}{2}[-\mathrm{i}J_m(kR) + Y_m(kR)]J_m(k\rho)\cos(m(\theta-\phi)), & R > \rho, \\ U^e(R,\theta;\rho,\phi) = \sum_{m=-\infty}^{\infty} \frac{\pi}{2}[-\mathrm{i}J_m(k\rho) + Y_m(k\rho)]J_m(kR)\cos(m(\theta-\phi)), & R < \rho, \end{cases} \tag{6}$$

$$T(s,x) = \begin{cases} T^i(R,\theta;\rho,\phi) = \sum_{m=-\infty}^{\infty} \frac{\pi k}{2}[-\mathrm{i}J'_m(kR) + Y'_m(kR)]J_m(k\rho)\cos(m(\theta-\phi)), & R > \rho, \\ T^e(R,\theta;\rho,\phi) = \sum_{m=-\infty}^{\infty} \frac{\pi k}{2}[-\mathrm{i}J_m(k\rho) + Y_m(k\rho)]J'_m(kR)\cos(m(\theta-\phi)), & R < \rho, \end{cases} \tag{7}$$

$$L(s,x) = \begin{cases} L^i(R,\theta;\rho,\phi) = \sum_{m=-\infty}^{\infty} \frac{\pi k}{2}[-\mathrm{i}J_m(kR) + Y_m(kR)]J'_m(k\rho)\cos(m(\theta-\phi)), & R > \rho, \\ L^e(R,\theta;\rho,\phi) = \sum_{m=-\infty}^{\infty} \frac{\pi k}{2}[-\mathrm{i}J'_m(k\rho) + Y'_m(k\rho)]J_m(kR)\cos(m(\theta-\phi)), & R < \rho, \end{cases} \tag{8}$$

$$M(s,x) = \begin{cases} M^i(R,\theta;\rho,\phi) = \sum_{m=-\infty}^{\infty} \frac{\pi k^2}{2}[-\mathrm{i}J'_m(kR) + Y'_m(kR)]J'_m(k\rho)\cos(m(\theta-\phi)), & R > \rho, \\ M^e(R,\theta;\rho,\phi) = \sum_{m=-\infty}^{\infty} \frac{\pi k^2}{2}[-\mathrm{i}J'_m(k\rho) + Y'_m(k\rho)]J'_m(kR)\cos(m(\theta-\phi)), & R < \rho, \end{cases} \tag{9}$$

where $x = (\rho,\phi)$, $s = (R,\theta)$, J_m and Y_m are the first and second Bessel functions with order m, respectively. It is found that the source and field points are separated in the degenerate kernels of Eqs. (6)–(9). For the boundary densities, u and t, on the circular boundary, we have

$$u(\theta) = a_0 + \sum_{n=1}^{\infty}(a_n\cos n\theta + b_n\sin n\theta), \quad 0 \leqslant \theta < 2\pi, \tag{10}$$

$$t(\theta) = p_0 + \sum_{n=1}^{\infty}(p_n\cos n\theta + q_n\sin n\theta), \quad 0 \leqslant \theta < 2\pi, \tag{11}$$

where a_0, a_n, b_n, p_0, p_n and q_n are the Fourier coefficients for u and t, respectively. For the Dirichlet case, a_0, a_n and $b_n (n \geqslant 1)$ are known, while p_0, p_n and $q_n (n \geqslant 1)$ need to be determined. By adopting the null-field equation, we have

$$0 = \int_B T^i(s,x)u(s)\,\mathrm{d}B(s) - \int_B U^i(s,x)t(s)\,\mathrm{d}B(s), \quad x \in \overline{D}, \tag{12}$$

where $\overline{D}$ is outside the domain of interest D. By substituting the series forms for the kernels of Eqs. (6) and (7) and the boundary densities of Eqs. (10) and (11) into Eq. (12) and using the orthogonal properties of Fourier bases, we have

$$p_0 = -\frac{H_0^{(1)'}(ka)J_0(ka)}{H_0^{(1)}(ka)J_0(ka)}a_0 k, \tag{13}$$

$$p_m = -\frac{H_m^{(1)'}(ka)J_m(ka)}{H_m^{(1)}(ka)J_m(ka)}a_m k, \quad m \geqslant 1, \tag{14}$$

$$q_m = -\frac{H_m^{(1)'}(ka)J_m(ka)}{H_m^{(1)}(ka)J_m(ka)}b_m k, \quad m \geqslant 1, \tag{15}$$

where $H_m^{(1)}$ denotes the first kind Hankel function with order m. By substituting all the boundary unknowns into the field equation, we have

$$\begin{aligned} u(\rho,\phi) &= \sum_{m=0}^{\infty}\left(\frac{H_m^{(1)}(k\rho)}{H_m^{(1)}(ka)}\right)\left(\frac{J_m(ka)}{J_m(ka)}\right)(a_m\cos(m\phi) + b_m\sin(m\phi)) \\ &= \sum_{m=0}^{\infty}\left(\frac{H_m^{(1)}(k\rho)}{H_m^{(1)}(ka)}\right)\left(\frac{J_m(ka)}{J_m(ka)}\right)\sqrt{a_m^2 + b_m^2}\cos(m\phi - \tau), \quad \rho \geqslant a, \ 0 \leqslant \phi < 2\pi, \end{aligned} \tag{16}$$

after employing the following identities

$$H_m^{(1)}(ka) = J_m(ka) + \mathrm{i}Y_m(ka), \tag{17}$$

$$H_m^{(1)'}(ka) = J'_m(ka) + \mathrm{i}Y'_m(ka), \tag{18}$$

$$Y'_m(ka)J_m(ka) - \mathrm{i}Y_m(ka)J'_m(ka) = \frac{2}{\pi ka}, \tag{19}$$

where τ is the phase lag. By checking all the terms in the derivation, a term of zero divided by zero, $J_m(ka)/J_m(ka)$, can be found in Eqs. (13)–(16) for the case of irregular values such that $J_m(ka) = 0$. This motivates us to define the modal participation factor as $(H_m^{(1)}(k\rho)/H_m^{(1)}(ka))\sqrt{a_m^2 + b_m^2}$ for the term of numerical instability, $J_m(ka)/J_m(ka)$, with respect to the corresponding mode $\cos(m\phi - \tau)$. In a similar way, we can derive the modal participation factor, $(H_m^{(1)}(k\rho)/H_m^{(1)}(ka))\sqrt{a_m^2 + b_m^2}$, for the term of numerical instability, $J'_m(ka)/J'_m(ka)$, with respect to the corresponding mode $\cos(m\phi - \tau)$ in the *LM* method (hypersingular equation). Mathematically speaking, the irregular values can not result in any difficulty since the term of zero divided by zero can be directly determined by the L'Hospital's rule. In an easier way, the same two zero terms can be cancelled out straight forward. However, this is not the case in the real calculation since the unknown densities are assumed in a separate way.

4. Modal participation factor for numerical instability—discrete system

In this section, the modal participation factor for numerical instability resulted from the fictitious frequencies is derived for a discrete system with an arbitrary boundary. By discreting $2N$ boundary elements along the boundary and using the SVD technique for U and T matrices in Eq. (3), we have

$$\Phi_U \Sigma_U \Psi_U^{\dagger} t = \Phi_T \Sigma_T \Psi_T^{\dagger} u, \tag{20}$$

where $\dagger$ denotes the transpose conjugate, Φ_U, Ψ_U, Φ_T and Ψ_T are the unitary matrices, Σ_U and Σ_T are the diagonal matrices composed by the singular values $\sigma_i^{(U)}$ and $\sigma_i^{(T)}$ of U and T matrices, respectively. By choosing the $2N$ column vectors in Ψ_U and Ψ_T as bases for t and u, respectively, we have

$$t = \Psi_U \alpha = \sum_{n=-(N-1)}^{N} \alpha_n \psi_n^{(U)}, \tag{21}$$

and

$$u = \Psi_T \beta = \sum_{n=-(N-1)}^{N} \beta_n \psi_n^{(T)}, \tag{22}$$

where α and β are the generalized coordinates. By substituting Eqs. (21) and (22) into Eq. (20), we have

$$\Phi_U \Sigma_U \alpha = \Phi_T \Sigma_T \beta, \tag{23}$$

after using the unitary properties for Ψ_U and Ψ_T. When k is a fictitious frequency (k_f), there exists a $\phi_i^{\dagger}$ which satisfies

$$\begin{bmatrix} U^{\dagger}(k_f) \\ T^{\dagger}(k_f) \end{bmatrix} \phi_i = 0, \tag{24}$$

after using the Fredholm alternative theorem. By taking the transpose conjugate with respect to Eq. (24), we have

$$\phi_i^{\dagger} [\, U(k_f) \quad T(k_f) \,] = 0. \tag{25}$$

Eqs. (24) and (25) are found to be the SVD updating terms and documents (Chen et al., 1999), respectively. By premultiplying $\phi_i^{\dagger}$ with respect to the left hand side and right hand side of the equal sign in Eq. (23), we have

$$\phi_i^{\dagger} \Phi_U \Sigma_U \alpha = \phi_i^{\dagger} \Phi_T \Sigma_T \beta. \tag{26}$$

For simplicity of demonstrable purpose, the Dirichlet problem is considered here. Eq. (26) is reduced to

$$\alpha_i = \frac{\sigma_i^{(T)}}{\sigma_i^{(U)}} \beta_i, \quad i \text{ no sum}, \tag{27}$$

since ϕ_i is one of the column vectors in Φ_U and Φ_T. By checking the terms in Eq. (27), an undeterminate term of zero divided by zero, $\sigma_i^{(T)}/\sigma_i^{(U)}$, can be found when k is an irregular value which satisfies $\sigma_i^{(T)} = \sigma_i^{(U)} = 0$. The modal participation factor can be defined as $(\sigma_i^{(T)}/\sigma_i^{(U)})\beta_i$ for the numerical instability, with respect to the corresponding mode $\psi_i^{(T)}$ instead of $\phi_i^{(T)}$. In the same way, we can derive the modal participation factor, $(\sigma_i^{(M)}/\sigma_i^{(L)})\beta_i$, with respect to the corresponding mode $\psi_i^{(M)}$ instead of $\phi_i^{(M)}$ in the *LM* method. By considering the special case of a circular radiator with ZN elements, Eq. (20) reduces to

$$\Phi H J \Psi^{\dagger} t = \Phi H' J \Psi^{\dagger} u, \tag{28}$$

where

$$\Phi = \Psi = \frac{1}{\sqrt{2N}} \begin{bmatrix} 1 & (e^{i\frac{2\pi}{2N}})^0 & (e^{-i\frac{2\pi}{2N}})^0 & \cdots & (e^{i\frac{2N\pi}{2N}})^0 \\ 1 & (e^{i\frac{2\pi}{2N}})^1 & (e^{-i\frac{2\pi}{2N}})^1 & \cdots & (e^{i\frac{2N\pi}{2N}})^1 \\ \vdots & \vdots & \vdots & \vdots & \vdots \\ 1 & (e^{i\frac{2\pi}{2N}})^{2N-2} & (e^{-i\frac{2\pi}{2N}})^{2N-2} & \cdots & (e^{i\frac{2N\pi}{2N}})^{2N-2} \\ 1 & (e^{i\frac{2\pi}{2N}})^{2N-1} & (e^{-i\frac{2\pi}{2N}})^{2N-1} & \cdots & (e^{i\frac{2N\pi}{2N}})^{2N-1} \end{bmatrix}_{2N\times 2N}, \tag{29}$$

$$H = \begin{bmatrix} H_0^{(1)}(ka) & 0 & 0 & \cdots & 0 \\ 0 & H_{-1}^{(1)}(ka) & 0 & \vdots & 0 \\ 0 & 0 & H_1^{(1)}(ka) & \vdots & 0 \\ \vdots & \vdots & 0 & \ddots & 0 \\ 0 & 0 & 0 & 0 & H_N^{(1)}(ka) \end{bmatrix}_{2N\times 2N}, \tag{30}$$

$$J = \begin{bmatrix} J_0(ka) & 0 & 0 & \cdots & 0 \\ 0 & J_{-1}(ka) & 0 & \vdots & 0 \\ 0 & 0 & J_1(ka) & \vdots & 0 \\ \vdots & \vdots & 0 & \ddots & 0 \\ 0 & 0 & 0 & 0 & J_N(ka) \end{bmatrix}_{2N\times 2N}. \tag{31}$$

In a similar way, we can obtain the modal participation factor for each mode using the *UT* and *LM* methods as shown in Tables 1 and 2, respectively.

Table 1
The modal participation factor in the *UT* method (singular equation)

Mode	Participation factor
ψ_0	$\frac{H_0^{(1)'}(ka)}{H_0^{(1)}(ka)}\frac{J_0(ka)}{J_0(ka)}\beta_0$
ψ_{-1}	$\frac{H_{-1}^{(1)'}(ka)}{H_{-1}^{(1)}(ka)}\frac{J_{-1}(ka)}{J_{-1}(ka)}\beta_{-1}$
ψ_1	$\frac{H_1^{(1)'}(ka)}{H_1^{(1)}(ka)}\frac{J_1(ka)}{J_1(ka)}\beta_1$
$\vdots$	$\vdots$
$\psi_{-(N-1)}$	$\frac{H_{-(N-1)}^{(1)'}(ka)}{H_{-(N-1)}^{(1)}(ka)}\frac{J_{-(N-1)}(ka)}{J_{-(N-1)}(ka)}\beta_{-(N-1)}$
$\psi_{(N-1)}$	$\frac{H_{(N-1)}^{(1)'}(ka)}{H_{(N-1)}^{(1)}(ka)}\frac{J_{(N-1)}(ka)}{J_{(N-1)}(ka)}\beta_{(N-1)}$
ψ_N	$\frac{H_N^{(1)'}(ka)}{H_N^{(1)}(ka)}\frac{J_N(ka)}{J_N(ka)}\beta_N$

Where $\psi_0, \psi_{-1}, \psi_1, \psi_{-2}, \ldots, \psi_{-(N-1)}, \psi_{(N-1)}$ and ψ_N are the $2N$ columns in $\Psi_{2N\times 2N}$ matrices.

Table 2
The modal participation factor in the *LM* method (hypersingular equation)

Mode	Participation factor
ψ_0	$\frac{H_0^{(1)'}(ka)}{H_0^{(1)}(ka)}\frac{J_0'(ka)}{J_0'(ka)}\beta_0$
ψ_{-1}	$\frac{H_{-1}^{(1)'}(ka)}{H_{-1}^{(1)}(ka)}\frac{J_{-1}'(ka)}{J_{-1}'(ka)}\beta_{-1}$
ψ_1	$\frac{H_1^{(1)'}(ka)}{H_1^{(1)}(ka)}\frac{J_1'(ka)}{J_1'(ka)}\beta_1$
$\vdots$	$\vdots$
$\psi_{-(N-1)}$	$\frac{H_{-(N-1)}^{(1)'}(ka)}{H_{-(N-1)}^{(1)}(ka)}\frac{J_{-(N-1)}'(ka)}{J_{-(N-1)}'(ka)}\beta_{-(N-1)}$
$\psi_{(N-1)}$	$\frac{H_{(N-1)}^{(1)'}(ka)}{H_{(N-1)}^{(1)}(ka)}\frac{J_{(N-1)}'(ka)}{J_{(N-1)}'(ka)}\beta_{(N-1)}$
ψ_N	$\frac{H_N^{(1)'}(ka)}{H_N^{(1)}(ka)}\frac{J_N'(ka)}{J_N'(ka)}\beta_N$

5. Numerical examples

Case 1. A radiation problem (Dirichlet condition)

For the first example, a radiation problem is considered. The governing equation and boundary condition are shown in Fig. 1. The normalized analytical solution to this cylinder problem of a radius a is

$$u(\rho,\phi)=\frac{H_4^{(1)}(k\rho)}{H_4^{(1)}(ka)}\cos(4\phi),\quad \rho\geqslant a,\quad 0\leqslant\phi<2\pi, \tag{32}$$

subject to boundary condition $u(a,\phi)=\cos(4\phi)$, where $H_4^{(1)}(k\rho)$ denotes the first-kind Hankel function of the fourth order. Fig. 2 shows the contour plot for the real-part solutions of $ka=1$. The positions where the irregular values occur can be found in Fig. 3 for the solution $t(a,0)$ versus k by using either the *UT* or the *LM* equation only. It is found that no irregular values can be found between zero to seven since the modal participation factors in the range are all zeros. At the position of $ka\approx 7.6$, the numerical instability appear since the value is the first zero of $J_4(ka)$ with nonzero participation factor for the *UT* method.

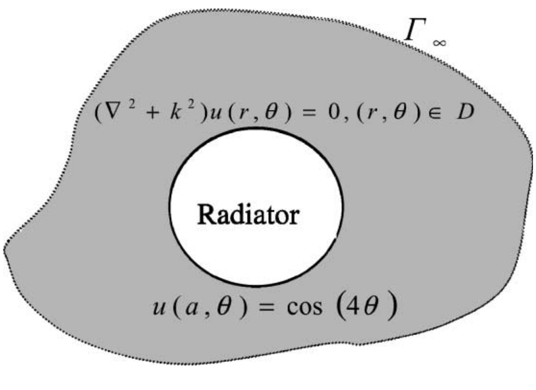

Fig. 1. The uniform radiation problem (Dirichlet condition) for a cylinder.

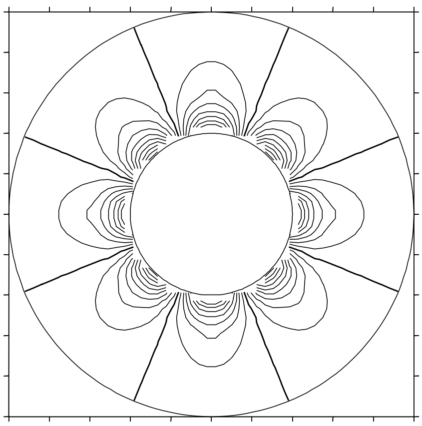

Fig. 2. The contour plot for the real-part solutions ($ka = 1.0$).

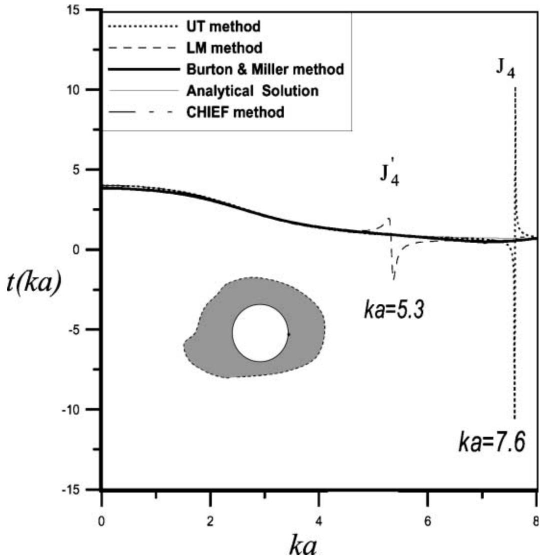

Fig. 3. The positions of irregular values using different methods.

Similarly, the irregular value occurs at $ka \approx 5.3$ since the value is the first zero of $J_4'(ka)$ with nonzero participation factor for the *LM* method. The *UT* and *LM* results agree well as shown in Fig. 3 except at the irregular values. The performance of the dual BEM in comparison with the analytical solution, the CHIEF method, and the Burton and Miller approach is quite good. For engineering applications, the CHIEF method may be the first choice for the practical engineers due to its simplicity. For the academic point of view, the Burton and Miller approach can avoid the fictitious frequency in a unified manner without taking any risk of failure.

Case 2. Nonuniform radiation problem (Neumann condition)

In order to clarify how modal participation factor dominates the numerical instability near the fictitious frequencies, the second example with the nonuniform Neumann boundary condition is designed in Fig. 4. The analytical solution is

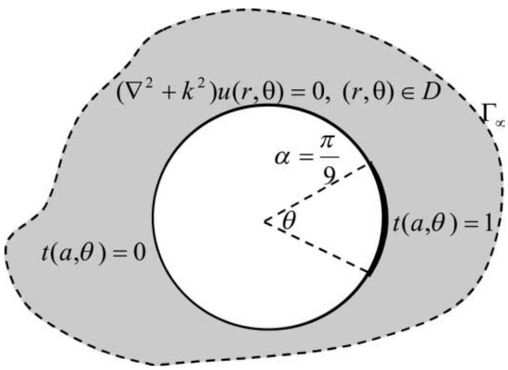

Fig. 4. The nonuniform radiation problem (Neumann condition) for a cylinder.

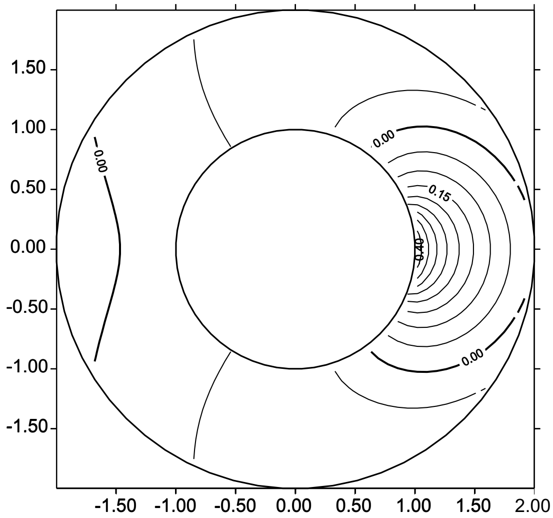

Fig. 5. The contour plot for the real-part solutions ($ka=1,\alpha=\frac{\pi}{9}$).

$$u(\rho,\phi)=\frac{1}{\pi}\frac{-\alpha}{k}\frac{H_0^{(1)}(k\rho)}{H_0^{(1)'}(ka)}+\frac{2}{\pi}\sum_{n=1}^{\infty}\frac{-1}{k}\frac{\sin(n\alpha)}{n}\frac{H_n^{(1)}(k\rho)}{H_n^{(1)'}(ka)}\cos(n\phi),\quad \rho\geqslant a,\ \ 0\leqslant\phi<2\pi. \tag{33}$$

Fig. 5 shows the contour plot for the real-part solutions. The irregular frequencies can be clearly found in Fig. 6 since the modal participation factor is not zero due to nonuniform excitation. Both the J_n and J_n' zeros are found. It indicates that numerical results agree well with the analytical solution except at the irregular positions using either the *UT* or *LM* method.

Case 3. Scattering problem (Dirichlet condition)

In order to check the validity of the program for scattering problem, example 3 is considered. The incident wave is plane wave and the object is a soft cylinder as shown in Fig. 7. The analytical solution for the scattering field is

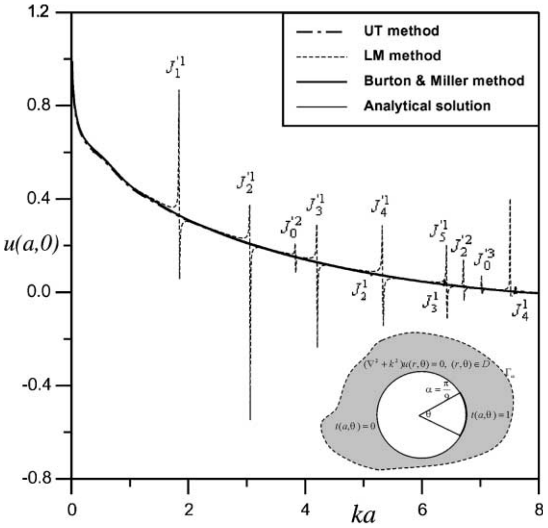

Fig. 6. The positions of irregular values using different methods.

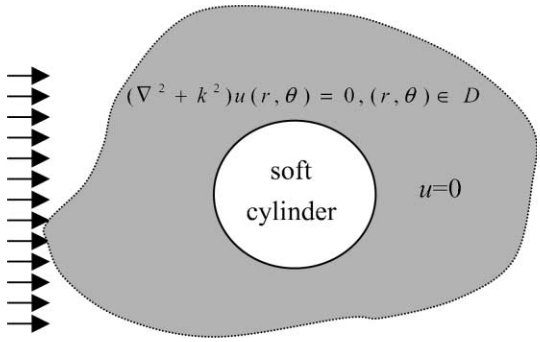

Fig. 7. The scattering problem (Dirichlet condition) for a cylinder.

$$u(\rho,\phi) = -\frac{J_0(ka)}{H_0^{(1)}(ka)} H_0^{(1)}(k\rho) - 2\sum_{n=1}^{\infty} i^n \frac{J_n(ka)}{H_n^{(1)}(ka)} H_n^{(1)}(k\rho)\cos(n\phi), \quad \rho \geqslant a, \ 0 \leqslant \phi < 2\pi. \tag{34}$$

Fig. 8 shows the contour plots for the real-part solutions. The positions where the irregular values occur can be found in Fig. 9 for the solution $t(a,0)$ versus k by using either the *UT* or the *LM* equation only. It is found that irregular values occur at J_n^m, the mth zeros of $J_n(ka)$ for the *UT* formulation, while the *LM* formulation has the irregular values of $J_n'^m$, the mth zeros of $J_n'(ka) = 0$. In comparing Fig. 9 with Fig. 6, it indicates that the irregular values are dominated by the chosen method, instead of boundary condition and problem types. In Fig. 9, it is found that irregular values of $J_n'^m$ are more evident than J_n^m after comparing with the modal participation factors in Tables 1 and 2. The Burton and Miller formulation and the CHIEF approach are employed to avoid the numerical resonance and the *UT* and *LM* results agree well except at the irregular wave numbers as shown in Fig. 9. The performance of the dual BEM in comparison with the analytical solution of Eq. (34) and the DtN results (Harari et al., 1997) is acceptable.

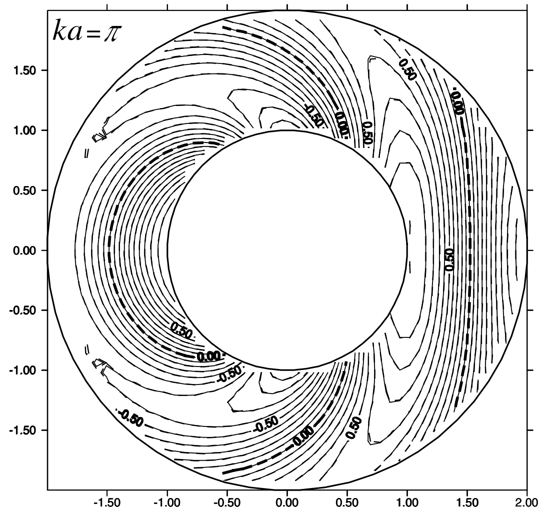

Fig. 8. The contour plot for the real-part solutions (analytical solution: dashed line, numerical result: solid line).

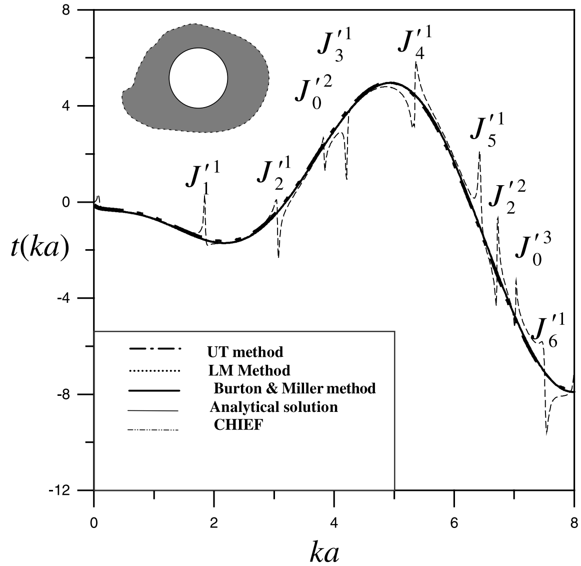

Fig. 9. The positions of irregular values using different methods.

Case 4. Scattering problem (Neumann condition)

In order to clarify how the irregular frequencies depend on the types of boundary conditions, the fourth example with the Neumann boundary condition is designed. The soft scatter in Example 3 is replaced by a rigid one in Fig. 10 with the following analytical solution

$$u(\rho,\phi) = -\frac{J_0'(ka)}{H_0^{(1)'}(ka)}H_0^{(1)}(k\rho) - 2\sum_{n=1}^{\infty} i^n \frac{J_n'(ka)}{H_n^{(1)'}(ka)}H_n^{(1)}(k\rho)\cos(n\phi), \quad \rho \geqslant a, \ \ 0 \leqslant \phi < 2\pi. \tag{35}$$

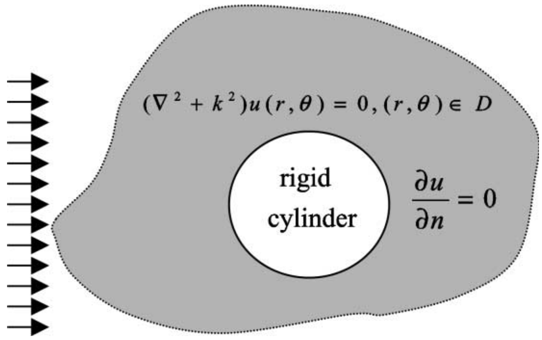

Fig. 10. The scattering problem (Neumann condition) for a cylinder.

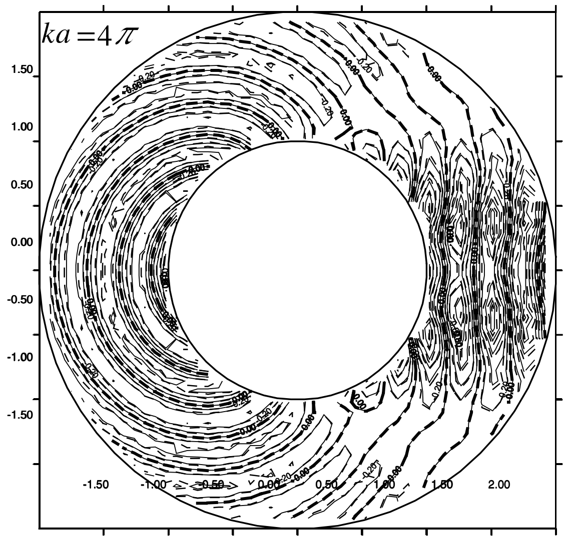

Fig. 11. The contour plot for the real-part solutions (analytical solution: dashed line, numerical results: solid line).

Fig. 11 shows the contour plots for the real-part solutions. The positions where the irregular values occur can be found in Fig. 12 for the solution $u(a, 0)$ versus k by using either the *UT* or the *LM* equation only. The performance of the *UT* and *LM* methods in comparison with the analytical solution of Eq. (35), the Burton and Miller solution, the CHIEF solution and the DtN results (Stewart and Hughes, 1997) is quite good except at the positions of irregular values where nonzero participation factors are predicted theoretically.

6. Concluding remarks

The mechanism why fictitious frequencies occur in the dual BEM has been examined by considering radiation and scattering problems of a cylinder. The concept of modal participation factor for continuous system and discrete system was proposed in a unified way by demonstrating a circular example. It is found that modal participation factor dominates the numerical instability near the irregular frequencies for the corresponding fictitious mode. The irregular values depend on the integral formulation, either the *UT*

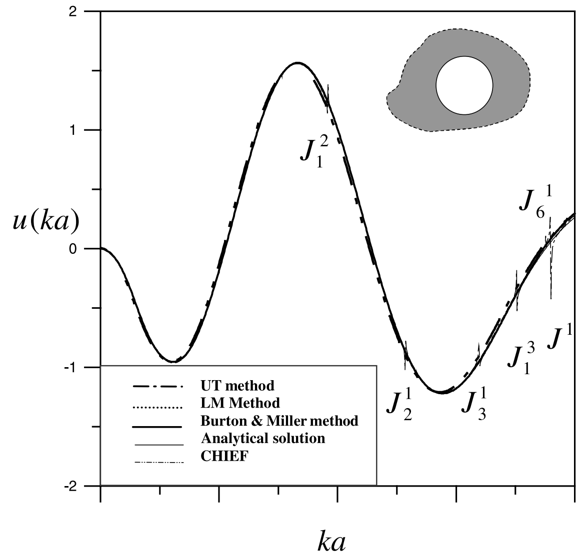

Fig. 12. The positions of irregular values using different methods.

(singular) or the *LM* (hypersingular) equation, instead of the types of boundary condition (Dirichlet or Neumann). Also, the radiation and scattering problems have the same fictitious frequencies once the method is chosen. The concept of zero modal participation factor can explain why the numerical instability near the predicted fictitious frequencies may not appear in the numerical experiments and was demonstrated in the numerical results. All the examples show that the singular (UT) equation results in fictitious frequencies at the zeros of $J_n(ka) = 0$, which are associated with the interior eigenfrequencies of essential homogeneous boundary conditions, while the hypersingular (LM) equation produces fictitious frequencies at the zeros of $J_n'(ka) = 0$, which are associated with the interior eigenfrequencies of natural homogeneous boundary conditions. The numerical results using the dual BEM program agree very well with the analytical solutions and the DtN results except at and near the irregular values. For comparisons, the Burton and Miller approach and the CHIEF method were successfully employed to deal with the problem of numerical instability near the fictitious frequency.

Acknowledgement

Financial support from the National Science Council, under grant no. NSC-91-2211-E-019-009, for National Taiwan Ocean University is gratefully acknowledged.

References

Burton, A.J., Miller, G.F., 1971. Proc. R. Soc. London Ser. A 323, 201.
Chen, J.T., 1998. Mech. Res. Commun. 25, 529.
Chen, J.T., Chen, C.T., Chen, K.H., Chen, I.L., 2000. Mech. Res. Commun. 27, 685.
Chen, I.L., Chen, J.T., Liang, M.T., 2001. J. Sound Vib. 248 (5), 809.
Chen, J.T., Chyuan, S.W., You, D.W., Wong, F.C., 1997. Finite Elements Anal. Des. 26, 129.
Chen, J.T., Hong, H.-K., Yeh, C.S., 1995. Commun. Numer. Meth. Engng. 11, 479.

Chen, J.T., Kuo, S.R., Cheng, Y.C., 1999. IUTAM/IACM/IABEM Symposium, Cracow.
Chen, J.T., Hong, H.-K., Yeh, C.S., Chyuan, S.W., 1996. Earthquake Eng. Struct. Dynam. 25, 909.
Chen, J.T., Kuo, S.R., 2000. Mech. Res. Comm. 27, 49.
Harari, I., Barbone, P.E., Montgomery, J.M., 1997. Int. J. Numer. Meth. Eng. 40, 2791.
Schenck, H.A., 1968. J. Acoust. Soc. Amer. 44 (1), 41.
Stewart, J.R., Hughes, T.J.R., 1997. Computer Methods Appl. Mech. Engng. 146, 65.